

EMBRYO IMPACTS AND GAS GIANT MERGERS. I. DICHOTOMY OF JUPITER AND SATURN'S CORE MASS

SHU LIN LI^{1,2}, C.B. AGNOR³, AND D. N. C. LIN^{2,4}

¹ Department of Astronomy, Kavli Institute of Astronomy and Astrophysics, Peking University, Beijing, China

² Department of Astronomy and Astrophysics, University of California Santa Cruz, USA

³ Astronomy Unit, School of Mathematical Sciences, Queen Mary University of London, UK

⁴ Kavli Institute of Astronomy and Astrophysics, Peking University, Beijing, China

Received 2009 May 11; accepted 2010 July 14; published 2010 August 18

ABSTRACT

Interior to the gaseous envelopes of Saturn, Uranus, and Neptune, there are high-density cores with masses larger than 10 Earth masses. According to the conventional sequential accretion hypothesis, such massive cores are needed for the onset of efficient accretion of their gaseous envelopes. However, Jupiter's gaseous envelope is more massive and its core may be less massive than those of Saturn. In order to account for this structural diversity and the super-solar metallicity in the envelope of Jupiter and Saturn, we investigate the possibility that they may have either merged with other gas giants or consumed several Earth-mass protoplanetary embryos during or after the rapid accretion of their envelope. In general, impinging sub-Earth-mass planetesimals disintegrate in gas giants' envelopes, deposit heavy elements well outside the cores, and locally suppress the convection. Consequently, their fragments sediment to promote the growth of cores. Through a series of numerical simulations, we show that it is possible for colliding super-Earth-mass embryos to reach the cores of gas giants. Direct parabolic collisions also lead to the coalescence of gas giants and merging of their cores. In these cases, the energy released from the impact leads to vigorous convective motion throughout the envelope and the erosion of the cores. This dichotomy contributes to the observed dispersion in the internal structure and atmospheric composition between Jupiter and Saturn and other gas giant planets and elsewhere.

Key words: planetary systems

Online-only material: color figures

1. INTRODUCTION

In the conventional sequential accretion hypothesis (SAH) for gas giant planet formation (Safronov 1969; Pollack et al. 1996), heavy elements first coagulate into planetesimals and protoplanetary embryos. When they attain a critical mass $M_{\text{crit}} \sim 3\text{--}10 M_{\oplus}$, they begin to accrete gas efficiently and to evolve into gas giants (Stevenson 1982; Bodenheimer & Pollack 1986).

Perhaps the strongest supports for SAH are the inferred existence of solid cores and super-solar metallicity in the envelopes of solar-system gas and ice giants (Guillot et al. 2004; Militzer et al. 2008). These models are constructed to match the observed masses, radii, and moments of inertial of present-day Jupiter, Saturn, Uranus, and Neptune.

Despite this verification, theoretical explanations are needed for two observed properties: (1) a significant difference in the core mass between Jupiter and Saturn and (2) the super-solar metallicity in the envelopes of gas giants. In Section 2, we discuss the uncertainties and pose challenges to the simplest version of SAH introduced by these two puzzles. We suggest that the dispersion in the core mass and the enhanced metallicity in the envelope of gas giants may be the consequence of some catastrophic collisional events which occurred well after the onset of efficient gas accretion. We discuss the common occurrence of giant impact and merger (GIM) events during the formation of isolated and multiple proto gas giants as well as throughout their long-term dynamical evolution.

We carry out numerical simulation to demonstrate that GIMs can indeed lead to diverse planetary structures. In Section 3, we briefly describe our numerical methods and discuss the typical range of appropriate orbital parameters and planetary properties. With a smoothed particle hydrodynamic (SPH) scheme, we illustrate the possibility that sufficiently massive protoplanetary

embryos may be able to intrude through the massive envelope and impact onto the cores of some gas giants. With three examples of head-on, parabolic collisions between a Saturn-like gas giant with super-Earth embryos and another gas giant, we show that spherical symmetry is quickly restored after the cores of the merger products are thoroughly mixed.

In order to extend the simulation to a larger dynamical range in density and over protracted phases of dynamical evolution, we construct a spherically symmetric Lagrangian hydrodynamic (LHD) scheme. With this LHD scheme, we consider, in Section 4, impactors with a range of masses and head-on collisional speeds. We show that low-velocity and low-mass impactors generally disintegrated in the gaseous envelope of gas giants and their debris has a tendency to sediment toward the planets' cores. Such events lead to the enlargement of the core mass. However, large-mass and high-speed impactors can survive their passage through the gaseous envelope and reach the gas giants' core. The dissipation of kinetic energy into internal energy induces efficient and vigorous thermal convection and erosion of the cores. These diverse outcomes may be responsible for introducing a variety of internal structure for long-period gas giants. In a follow-up paper II (S.-L. Li et al. 2010, in preparation), we will apply a similar scenario to a series of models for short period planets with diverse internal structures. Finally, we summarize our results in Section 5.

2. THE DIVERSE STRUCTURE OF GAS GIANTS DUE TO GIANT IMPACTS AND MERGERS DURING PROTOPLANETARY FORMATION

In the sequential accretion hypothesis collisions represent a principal mode of growth and planetary evolution. Giant planetary collisions have been suggested to explain a variety of bulk planetary characteristics in the solar system, including the

origin of Earth's Moon (Hartmann & Davis 1975; Cameron & Ward 1976), collisional stripping of Mercury's primordial mantle (Benz et al. 1988, 2007), and Uranus' large obliquity (Slattery et al. 1992). Giant impacts during the accretion epoch display a diversity of outcome morphologies, each with different implications for the development of planetary characteristics (e.g., Wetherill 1985; Agnor & Asphaug 2004; Asphaug et al. 2006). Recent studies have begun to explore how these energetic impacts influence the luminosity, detectability, and characteristics of extrasolar planets (Anic et al. 2007; Ikoma et al. 2006). Here, we build on these works and examine how giant planetary collisions may account for the diversity of the interior structure of gas giant planets and the differences in core mass between Jupiter and Saturn in particular.

In this section, we provide arguments to highlight the critical roles of giant impacts and mergers during the formation and evolution of gas giant planets and the potential outcomes of such events.

2.1. Observed Structural Diversity and its Paradoxical Implications

Although they are both classified as gas giants, Jupiter and Saturn have very different internal structures. Within considerable uncertainty, the estimated core mass of Saturn is more massive (by up to three times) than that of Jupiter. In contrast, Jupiter's total mass (which is mostly contained in its envelope) is around three times that of Saturn. The average metallicity of both planets is inferred to be several times that of the Sun, albeit they are unlikely to be identical.

According to SAH, gas giants acquired their cores prior to the accretion of their gaseous envelopes. Current quantitative models indicate that a critical core mass ($M_{\text{crit}} \sim 10 M_{\oplus}$) is needed for the onset of efficient accretion of the surrounding gas (Pollack et al. 1996). This mass is determined by the heat transfer efficiency (Inaba & Ikoma 2003) and the nebula boundary conditions (Bodenheimer et al. 2000; Wuchterl et al. 2000; Papaloizou & Terquem 2006; Rafikov 2006).

There are considerable uncertainties on the magnitude of M_{crit} . The first sets of quantitative models were constructed under the assumptions of spherical symmetry, hydrostatic equilibrium, efficient convection, interstellar-grain opacity, and idealized planetesimal bombardment rate (Pollack et al. 1996). These models indicate that uninterrupted planetesimal bombardments and a cooling barrier can delay the formation of Jupiter in a minimum mass nebula (MMN) by 10–20 Myr.

However, gas giants can only acquire their massive envelope inside gas-rich protostellar disks, i.e., their formation timescale τ_m must be smaller than the typical gaseous disk depletion timescale $\tau_{\text{dep}} (\sim 3\text{--}5 \text{ Myr})$. There have been several previous attempts to resolve this theoretical challenge. Alibert et al. (2004) suggested that type I migration of Earth-mass embryos (Ward 1997) may speed up the timescale needed for the onset of efficient gas accretion. Although this scenario may provide a solution for Saturn (because its core is relatively massive), it may not be appropriate for Jupiter if its core mass is limited to a few M_{\oplus} .

In an attempt to account for Jupiter's low-mass core, Inaba & Ikoma (2003) and Hubickyj et al. (2005) constructed models to show that the gas accretion rate increases with the heat transport efficiency. Since there are radiative regions in the envelopes of proto gas giants, the critical mass for the onset of efficient gas accretion increases with the opacity of the infalling envelope. The main sources of opacity in these regions are grains. Grain

growth and formation of planetesimals can reduce the opacity of residual disk gas substantially (see Section 2.2). It is also possible for dust to coagulate and sediment from the tenuous outer envelope of protoplanets (Helled et al. 2008).

In principle, these effects can suppress the barrier for the onset of gas accretion. However, a rich population of super-Earths (with masses $M_p >$ a few M_{\oplus}) has been discovered with radial-velocity (Mayor et al. 2009) and transit (Queloz et al. 2009) surveys. Some of these super-Earths have masses larger than Jupiter's estimated core mass (at least for some models). This discrepancy would introduce a paradox, if we assume that these super-Earths attained their present-day mass and became "failed cores" in gas-rich protostellar disks because their mass $M_p < M_{\text{crit}}$. It is possible that the onset of gas accretion onto these super-Earths may be delayed by planetesimal bombardment, albeit such events are likely to be suppressed by the formation of a gap in the planetesimal disk (see Section 2.4; Zhou & Lin 2007).

Although this accretion timescale issue is not the central focus of our discussion here, scenarios proposed for its resolution have implications which exacerbate the second paradox, i.e., gas giants' structural diversity. If the internal structure of the mature planets is assumed to be the result of some critical conditions that led to their formation, the large observed dispersion would imply the existence of many possible paths for their final assemblage.

For example, both Jupiter and Saturn probably formed in a similar solar nebula environment close to their present-day location (albeit at different times). It is natural to assume a similar magnitude for M_{crit} for the onset of efficient gas accretion, especially if their separation may have widened through planetesimal scattering since their formation (Hahn & Malhotra 1999). The dichotomy of their internal structure is indicative that it only partially reflects the critical initial condition for the onset of efficient gas accretion. It is entirely possible that the present-day internal structure of gas giants has been affected by some local or temporal stochastic processes after they have initiated (or terminated) the process of rapid accretion of their massive envelope.

2.2. Heavy Elemental Abundance in Gas Giants' Envelope

A related conundrum is the super-solar metallicity content of Jupiter and Saturn's gaseous envelopes. In the SAH, heavy elements are assumed to be mostly condensed into grains, efficiently segregated from the disk gas and converted into planetesimals, embryos, and cores prior to the onset of the gas accretion. The abundance distribution of refractory elements in the meteorites suggests that the solar nebula had an initial composition similar to that of the sun. The emergence of solid cores with $M_p > M_{\text{crit}}$ would decrease the nebula's overall metallicity, including contribution from molecules and grains. If gas giants' envelopes are composed solely of nebula gas and grains accreted by their cores, they would attain a sub-solar metallicity. This inference clearly contradicts with the observed super-solar metallicity in Jupiter and Saturn's envelopes.

One possible solution for this paradox is that Jupiter and Saturn formed in regions where heavy elements are locally enhanced. Due to hydrodynamic drag, grains formed in the outer disk regions migrate inward. They may stall and accumulate near the snow line (a_{ice} where the disk mid-plane temperature decreases below ice condensation temperature at 160 K; see e.g., Cuzzi & Zahnle 2004; Kretke & Lin 2007). This migration barrier to grains and embryos provides a preferred location for gas giants to assemble (Ida & Lin 2008) (see Section 2.3).

However, a strong metallicity enhancement would increase the effective opacity of gaseous envelopes around solid cores and the magnitude of M_{crit} (Inaba & Ikoma 2003) well beyond the current estimated core mass for Jupiter (Guillot et al. 2004; Militzer et al. 2008). Although coagulation and sedimentation of grains in protoplanets' envelopes may provide a potential solution for Jupiter's small core (Helled et al. 2008), it is not clear why such a process did not also enable Saturn to attain a small M_{crit} and low core mass.

Another possible cause of the high metallicity in gas giants' envelopes is the erosion of their cores. However, such a scenario would require much more massive cores (up to $\sim 30\text{--}50 M_{\oplus}$) prior to the onset of efficient gas accretion. In an MMN, formation of such massive embryos is challenging though not impossible. Core erosion by convective gas may also be suppressed by the compositional gradient in the boundary layer separating gas giants' cores and envelopes (Guillot et al. 2004). This scenario can also be easily ruled out by any dip in the planetary mass distribution in the range of $10\text{--}100 M_{\oplus}$ (Ida & Lin 2004).

2.3. Emergence of Cores of the First-generation Gas Giants

In this paper, we propose giant impacts of residual embryos onto gaseous planets during and after the advanced stages of their envelope accretion as a potential mechanism which may lead to the resolution of the structural diversity (see Section 2.1) and metal-rich envelope (see Section 2.2). In order to distinguish between the *ab initial* core and the giant-impact scenarios, we first discuss the dynamical evolution of massive embryos in the context of gas giant formation.

The growth of embryos is limited by their isolation mass (M_{iso} , see e.g., Lissauer 1987) and long growth timescale (τ_m ; Ida & Lin 2004). In an MMN-type protostellar disks, the most massive embryos emerge beyond a_{ice} within the gas depletion timescale (τ_{dep}) is $\sim 3\text{--}5 M_{\oplus} < M_{\text{crit}}$. Furthermore, the onset of gas giant formation is challenged by the type I orbital migration of their super-Earth embryonic cores. The rate and direction of type I migration are determined by both the surface density (Σ_g) and temperature T (more accurately the entropy) gradient in the disk gas (Masset et al. 2006; Paardekooper 2010). These quantities are determined by the efficiency of turbulent-induced angular momentum transport. Possible causes of turbulence include the magneto-rotational (MRI; Balbus & Hawley 1991) and convective (Lin & Papaloizou 1980; Lesur & Ogilvie 2010) instabilities.

Near the snow line of an MMN, the ionization fraction near the disk midplane is negligible and the gas there is unaffected by MRI turbulence. However, the ionization fraction may be much higher near the disk surface layers which are exposed to the ionizing photons from the central stars and elsewhere (Gammie 1996). The depth of layers which are affected by the MRI turbulence is determined by an ionization equilibrium in which the ionization rate is balanced by the rate of recombination on the grains. Interior to a_{ice} , the sublimation of volatile ices eliminates a majority of the recombination sites, enhances the ionization fraction of the disk gas, and increases the depth of the surface layer which is regulated by MRI turbulence. Across a_{ice} , effective viscosity has a negative gradient, which in quasi-steady state leads to a positive gradient in Σ_g and P_g . For a range of disk mass accretion rates ($\dot{M}_d \sim 10^{-9}\text{--}10^{-8} M_{\odot} \text{ yr}^{-1}$), the local P_g maximum at a_{ice} provides a natural barrier for the orbital decay of grains against hydrodynamic drag (Kretke & Lin 2007). This structure also reverses the direction of type I

migration due to the effect of horseshoe drag (Masset et al. 2006). Outward migration of embryos by a few AU may also be induced by an entropy gradient (Paardekooper 2010).

Thus, similar to grains' orbital evolution, embryos' migration leads them to congregate near a_{ice} where both the gas surface density (Σ_g) and pressure (P_g) attain local maxima in the disk due to the transition in the efficient turbulent angular momentum transport. Through the accumulation of neighboring embryos and planetesimals, a protoplanet may acquire sufficient mass (i.e., $\sim M_{\text{crit}}$) to evolve into a core which efficiently accretes gas (Ida & Lin 2008).

2.4. Embryos' Dynamical Evolution Around Isolated Gas Giants

During the early phase of gas accretion, the timescale for a protoplanet to double its mass is longer than the synodic periods (relative to its orbit) of planetesimals and embryos within its feeding zone. Its tidal perturbation on the nearby embryos and their interaction with the disk gas induce their orbit to evolve away from that of the dominant protoplanet (Zhou & Lin 2007; Shiraishi & Ida 2008). Therefore, slowly ("adiabatically") growing protoplanets cannot accrete those embryos within their expanding feeding zones in contrast to the assumption made in previous models (Pollack et al. 1996; Dodson-Robinson et al. 2008).

This initial suppression of giant impacts reduces the energy released by the growing protoplanet and promotes the gas accretion rate. In the limit of negligibly small thermal feedback and weak protoplanetary torque, protoplanets' uninhibited gas accretion rate (\dot{M}_p) may be approximated by the Bondi formula such that the mass doubling timescale would be

$$\tau_m \equiv \frac{M_p}{\dot{M}_p} \sim \left(\frac{M_*}{\pi \Sigma_g a^2} \right) \left(\frac{M_*}{M_p} \right) \left(\frac{H}{a} \right)^4 \frac{P}{2\pi}, \quad (1)$$

where H is the disk thickness.

The above expression indicates that, once it is initiated, Bondi-type gas accretion is a runaway process. During their growth, there are several effects which can lead to GIM events.

Effect 1. Proto gas giants' accretion rate \dot{M}_p is eventually suppressed by the structural changes in their natal disks induced by their tidal perturbation when their M_p exceeds $\sim (H/a)^3 M_*$, which is comparable to M_J in an MMN near a_{ice} (Dobbs-Dixon et al. 2007). However, just before they have acquired an adequate mass to induce gap formation, protoplanets' τ_m reduces below a thousand years (Tanigawa & Watanabe 2002), which is comparable to the synodic periods of their nearby planetesimals and embryos (with semimajor axis $a \pm \delta a \sim 0.1\text{--}0.2a$). Gas giants' rapid (non adiabatic) mass increases destabilize these embryos' orbits, and a modest fraction of these objects collide with and are captured by the emerging gas giants (Zhou & Lin 2007).

Effect 2. After gas giants' accretion is quenched by gap formation, their gravity perturbs the orbital elements of residual planetesimals and embryos out to quite large distances. To the lowest order, gas giants' secular perturbation leads to the modulation of the embryos' eccentricity and the precession of their longitude of periastron. The amplitude of embryos' eccentricity modulation increases with gas giants' eccentricity e_p and M_p (Murray & Holman 1999). Many known gas giants have significant e_p 's and they can induce modest amplitude eccentricity modulations among their nearby embryos.

The orbital precession frequency of embryos is determined by their a 's. Due to the self gravity of their natal disks, orbits of gas giants and residual embryos also precess with frequencies determined by their a 's relative to the $\Sigma_g + \Sigma_d$ distribution of the disk. Secular resonances occur at special locations where the embryos' precession frequencies due to the gravitational perturbation of the gas giants matches their differential precession frequencies due to the disk potential. In these resonances, embryos' eccentricities can be greatly excited by the nearly constant differential longitude of periastrons. During the depletion of the disk, gas giants' secular resonances sweep over wide regions and destabilize the orbits of the planetesimals and embryos at these locations (Ward 1981; Nagasawa et al. 2005; Thommes et al. 2008). Some embryos may cross the orbits of and collide with the gas giants.

2.5. GIMs in Systems with Multiple Gas Giants

There are two gas giants, Jupiter and Saturn, in the solar system. Several stars (such as ν And) have known multiple planets around them. Around other planet-bearing stars, there are indications of additional planetary companions with comparable M_p 's (Cumming et al. 2008). In these systems with multiple planets, there are several additional avenues which may lead to catastrophic impacts of residual embryos onto their envelopes. For example:

Effect 3. Regardless of the low formation and survival probability of the first-generation planets (Ida & Lin 2008), their birth leads to gap formation which provides a secondary pressure maximum in the gas disk outside their orbits (Lin & Papaloizou 1979, 1993; Bryden et al. 2000). This induced disk structure also sets up a barrier against the orbital decay of grains and embryos. The accumulation of heavy elements beyond the outer edge of the gap promotes the formation of more-distant second-generation cores on timescales much shorter than that required for them to assemble in isolation (Bryden et al. 2000). In this sequential formation scenario, the second-generation gas giants' rapid mass increase, during their advanced growth phase, also introduces non-adiabatic changes in the systems' gravitational potential which have a tendency to destabilize the orbits of the nearby residual embryos.

Effect 4. After the gas depletion, planets' orbits continue to evolve due to their scattering of residual planetesimals. If multiple planets' orbits have spread out from a more compact configuration, orbital instabilities and scattering amongst giant planets may also lead to late accretion of planetesimals by gas giants (Tsiganis et al. 2005).

2.6. Disruption of Impacting Embryos

The main focus of this paper is to examine the structure adjustment of gas giants' envelopes after major merger events rather than a statistical study on the coalescence probability. We do not consider collisions in which the intruding embryos pass through the envelope of gas giants without losing a significant fraction of their heavy elemental masses. For merger models, we choose a representative rather than a realistic distribution of models to illustrate the possibility and character (rather than probability) of two sets of outcomes, i.e., the intruding embryos either disintegrate in the gas giants' envelope or impact onto their cores.

For simplicity, we consider mostly head-on collisions. Impacting planetesimals much smaller than the giant planet would likely suffer ablative disintegration during their passage through

the gaseous envelope. On the other hand, sufficiently massive impactors may penetrate deep and reach the core. A projectile's disintegration becomes likely when it collides with an air-mass comparable to its own (Korycansky & Zahnle 2005). For head-on collisions, the distance traveled in a gas giant's envelope before disintegration is approximately $D \sim (\rho_e/\rho_g)R_e$ where ρ_e and ρ_g are the average density of the embryo and gas giant, and R_e is the radius of the embryo. Reaching the center of a planet ($D \gtrsim R_p$) requires a sufficiently large or massive impactor ($R_e/R_p \gtrsim (\rho_g/\rho_e)^3$). For Saturn-like gas giant planets ($\rho_g = 0.5\text{--}1.5 \text{ g cm}^{-3}$) hit by condensed rocky embryos ($\rho_e = 4\text{--}6 \text{ g cm}^{-3}$) reaching the core becomes feasible for impactors of $\sim M_\oplus$ or larger. We note that the length of the path to the core, the air-mass encountered, and hence the embryo mass required to reach it all depend on the impact orientation. Furthermore, the depth at which an impactor's mass and energy is deposited is sensitive to the impact orientation (Anic et al. 2007).

2.7. Mergers of Gas Giant Planets

In relatively massive disks, the formation of multiple systems may lead to merger events due to the following effects.

1. The emergence of the second-generation gas giants can perturb the orbit of their predecessors and induce them to undergo type III runaway migration (Masset 2008; Zhang & Hamilton 2007). During this phase of rapid orbital evolution, planets' orbits may be dynamically destabilized even though they are surrounded by considerable amount of disk gas (Zhou & Lin 2007, also see Section 2.4).
2. After the depletion of the disk gas, long-term dynamical instabilities induced by all the gas and ice giants on each other (and the embryos) can lead to their eccentricity excitation and orbit crossing (Duncan et al. 1987; Zhou et al. 2007) on a timescale

$$\log(T_c/P_k) = -5 + 2.2 k_0, \quad (2)$$

where P_k is the mean orbital period of the planets, $k_0 \simeq 2(q-1)a_i/(q+1)r'_H$, $q = a_{i+1}/a_i$ is the ratio of the semimajor axis between planets i and $i+1$, and the modified Hill's radius $r'_H = (M_p(a_i) + M_p(a_{i+1}))/3 M_*$ takes into account the mass of two interacting protoplanets (Zhou et al. 2007).

3. Eccentricity growth and orbit crossing widen planets' feeding zones but reduce their collisional cross sections to its geometric values. Close encounters can eventually lead to velocity dispersions comparable to the planets' surface escape speed V_{esc} . Interior to the region where the planets' Keplerian orbital velocity $V_{\text{kep}} \sim V_{\text{esc}}$, they undergo repeated close encounters until they eventually collide with each other (Lin & Ida 1997).

3. MODELS OF GIANT IMPACTS ONTO GAS GIANT PLANETS

Having established that GIMs are expected to commonly occur among long-period gas giants, we use two methods to simulate giant impacts between gas giants and planetesimals and mergers between two planets. In the first method, we model collisions into gas giant planets using SPH. It is a Lagrangian particle method suitable for modeling highly deformed flows and shocks evolving in three dimensions. Because it only tracks material particles of interest, modeling flows into empty space

can be done economically without the need for including vast volumes of all potentially occupied space as in a grid type code. This versatile boundary-free multi-dimensional hydrodynamic scheme is well suited for the simulations of colliding astrophysical and planetary bodies.

A few dynamical times after a giant impact, the gross deformation gravitationally settles back to a new roughly symmetrical equilibrium shape. Over short timescales and for densities near that of the planet, the SPH model provides a good description of the planetary response. We examine the long-term thermal adjustment of the gaseous envelope using a one-dimensional (spherically symmetric) Lagrangian radiative hydrodynamic scheme.

3.1. Three-dimensional Smoothed Particle Hydrodynamic Models

SPH is widely used for modeling flows in a variety of astrophysical and planetary contexts (see, e.g., Monaghan 1992; Benz 1990, for reviews of the method). It has been used for a variety of problems including modeling stellar collisions (e.g., Benz & Hills 1987) as well as impacts between condensed solar system objects (Benz et al. 1986; Love & Ahrens 1996; Benz & Asphaug 1999; Asphaug et al. 1998). The model we use here employs a hierarchical tree to compute self-gravity and is a variant of the code used in Benz et al. (1986).

To simulate impacts into gas giant planets with cores, we must model the hydrodynamic response of both condensed and gaseous matter. We construct model planets using the Tillotson (Tillotson 1962) equation of state (see Appendix II of Melosh 1989) with the material parameters of iron to simulate the structure of the condensed core. The algebraic expression of this equation of state is convenient for use in SPH schemes.

We treat the giant planet’s gaseous envelope using a perfect gas equation of state, i.e., $P_g = (\gamma - 1)\rho u$ where P_g , ρ , and u are the pressure, density, and specific internal energy, respectively, and we have used $\gamma = 5/3$. Gas giant planetary models are constructed by surrounding an iron core with a gaseous envelope and letting the system relax to a state of hydrostatic equilibrium. In regions with modest density, the smoothing length is adjusted to maintain a specific number of neighbors. For numerical convenience, we employ a lower limit on the density of $\rho_l = 0.5 \text{ g cm}^{-3}$ such that the expansion of the smoothing length is suppressed for particles with density below this value. This density “floor” prevents gas in the individual fragments (or the envelope) from dispersing and diffusing out to tenuous medium. Since there is limited envelope expansion and very little mass loss associated with models presented here, this numerical prescription does not affect our results.

Finally, we model large planetary impactors using the Tillotson material parameters for both iron and basalt. In principle, impactors might be primarily composed of water ice. Impactors’ composition for a given mass can determine whether they disintegrate or impact onto the core. As we are simply interested in illustrating the gross characteristics of merger events (rather than numerically measuring the critical impactor mass or impact parameter which determine specific outcomes) our main conclusions are not strongly tied to the particular material properties chosen (e.g., basalt, iron, and ices) or the use of head-on versus the more common oblique collisions for particular impact models.

As discussed in Section 2, impactors into gas giant planets range from planetesimals and embryos to full grown planets. To explore a few of these possibilities, we have performed three

Table 1

Simulations of Collisions Between the Saturn-like Gas Giant and Embryos with Masses of $25 M_\oplus$ and $10 M_\oplus$ and Another Identical Saturn-mass Gas Giant, which are Denoted as Model a, b, and c, Respectively

Model	M_T (M_\oplus)	$M_{T,c}$ (M_\oplus)	M_I (M_\oplus)	$M_{I,c}$ (M_\oplus)	$M_{f,c}$ (M_\oplus)	$M_{f,g}$ (M_\oplus)	R_f/R_i
Sa	100	10	25	25	35	90	1.08
Sb	100	10	10	10	20	90	1.06
Sc	100	10	100	10	20	180	1.25
La	100	10	25	25	35	90	1.02
Lb	100	10	10	10	20	90	0.996
Lc	100	10	100	10	20	180	1.59

Notes. The models named as “S” correspond to the SPH calculations, while those named as “L” correspond to the one-dimensional LHD calculations. All the models are for parabolic, head-on, low-speed collisions. For the composition of the impactors, the embryos are made of Tillotson basalt, and the gas giant contains a $10 M_\oplus$ iron core and a $90 M_\oplus$ gaseous envelope. Quantities M_T , $M_{T,c}$, M_I , $M_{I,c}$, $M_{f,c}$, and $M_{f,g}$ correspond to the target’s total mass, its core mass, impactor’s total mass, its core mass, the planet’s final mass in the core, and gaseous envelope, respectively. Planets’ initial and asymptotic radii when a quasi-hydrostatic equilibrium is re-established after the GIMs are represented by R_i and R_f , respectively.

SPH simulations of impacts into a “Saturn-like” gas giant planet of mass $M_T = 100 M_\oplus$ which includes an iron core with a mass $M_{T,c} = 10 M_\oplus$. The first and second models are designed to consider the effects of giant impacts onto a gas giant planet by a planetary impactor with $M_I = 10 M_\oplus$ and $M_I = 25 M_\oplus$, respectively. The impactor is assumed to be entirely made of basalt such that its core mass $M_{I,c} = M_I$. A third model examines the merger of two gas giants each with $M_T = 100 M_\oplus$ and $M_{T,c} = 10 M_\oplus$.

For long-period planets, it is not likely for the high-velocity collisions to occur. Therefore, we set the impact speed $v_{\text{imp}} = v_{\text{esc}}$, where the two-body escape velocity is $v_{\text{esc}} = (2G(M_I + M_T)/(R_I + R_T))^{1/2}$ for the models in this paper. Model parameters and results of these simulations are summarized as “S” series in Table 1.

As expected in relatively low-speed, parabolic collisions, the impactor always merges with and is consumed by the gas giants. The gross morphology of the collision product and the delivery of the impactor mass and energy into the giant planet are illustrated in snapshots of the Sb model shown in Figure 1.

During the initial stages of collision, the impactor excavates a crater in the gas giant’s envelope. Over a few dynamical times the initial deformation propagates throughout the planet and the body begins oscillating globally and relaxing as the impactor travels to the planet’s center. In the course of this passage, the impactor is flattened and sheds mass before eventually reaching the core. As discussed above, a $10 M_\oplus$ impactor is sufficiently massive that a significant fraction of its initial mass reaches the core at once. The impactor then equilibrates with the core, material settles back into a new state of hydrostatic equilibrium, and the planet assumes the expected larger spherically symmetric shape.

A portion of the impactor and impact energy are deposited high up in the gaseous envelope. Eventually sedimentation of this mass may release additional energy on a much longer timescale. While the precise partitioning depends on impactor mass, velocity, and orientation, it is clear that large impacts can deposit mass and energy in large parcels into both the core and envelope.

In addition, the final volumetric radius of the SPH result is in good agreement with those of our one-dimensional LHD

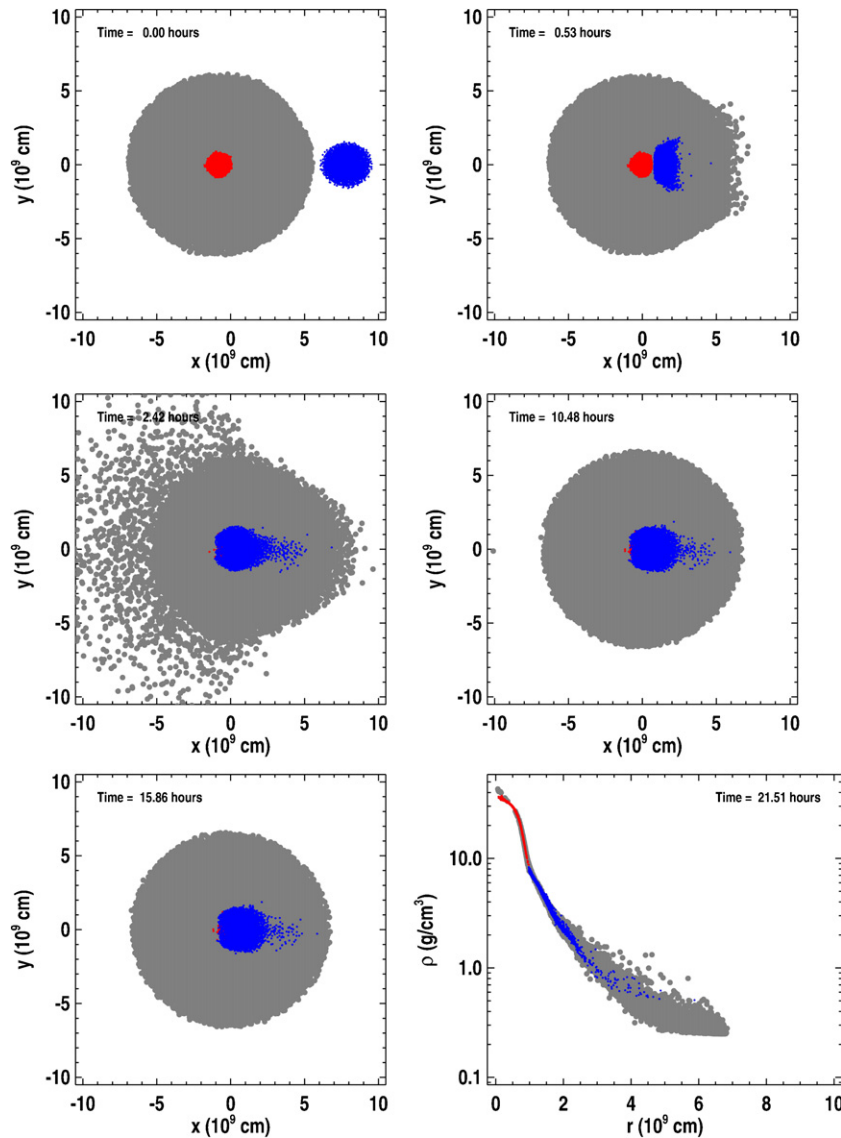


Figure 1. Collision between a Saturn-like gas giant and a $10 M_{\oplus}$ impactor (Run Sb). Gas particles are shown as gray. Core particles are overplotted in red, and the basalt impactor is overplotted in blue.

(A color version of this figure is available in the online journal.)

model (see below) suggesting that longer term thermal evolution may be encapsulated using a more computationally convenient approach.

3.2. The One-dimensional Lagrangian Radiative Hydrodynamic Impact Model

The 3D-SPH scheme is not ideally suited for the demanding computation of the long-term evolution of the gas giant planets. The results generated from the preliminary SPH scheme indicate that internal flow quickly isotropizes the density distribution of the merger product (see below). In the limit of negligible rotation, the structural response and evolution of the envelope, due to the release of thermal energy during the core coalescence, can be computed with a one-dimensional LHD scheme. This approach was firstly adopted by Wuchterl (1991) in his calculation of the planet formation problem. Although a similar approach is used, our independently developed LHD scheme is based on a more conventional prescription for the convective heat transfer and an alternative approximation for the computation of the thermal evolution of planets (see Section 3.2.2).

3.2.1. Governing Equations for the LHD Scheme

The basic equations for the LHD scheme include three conservation laws of momentum, mass, and energy, and the equation of state for the relationship among the thermodynamical quantities. When writing them in the Lagrangian scheme, these equations are as follows:

$$\frac{\partial u}{\partial t} = -\frac{1}{\rho_0} \left(\frac{R(r, t)}{r} \right)^2 \frac{\partial(P+q)}{\partial r} + \frac{\partial\Psi}{\partial r} \quad (3)$$

$$\frac{\partial R}{\partial t} = u \quad (4)$$

$$\frac{1}{\rho} = \frac{1}{\rho_0} \left(\frac{R(r, t)}{r} \right)^2 \frac{\partial R}{\partial r} \quad (5)$$

$$\frac{\partial \varepsilon}{\partial t} = \left(\frac{P+q}{\rho^2} \right) \frac{\partial \rho}{\partial t} - \frac{1}{\rho} \nabla \cdot \vec{F} \quad (6)$$

$$\varepsilon = f(P, \rho), \quad (7)$$

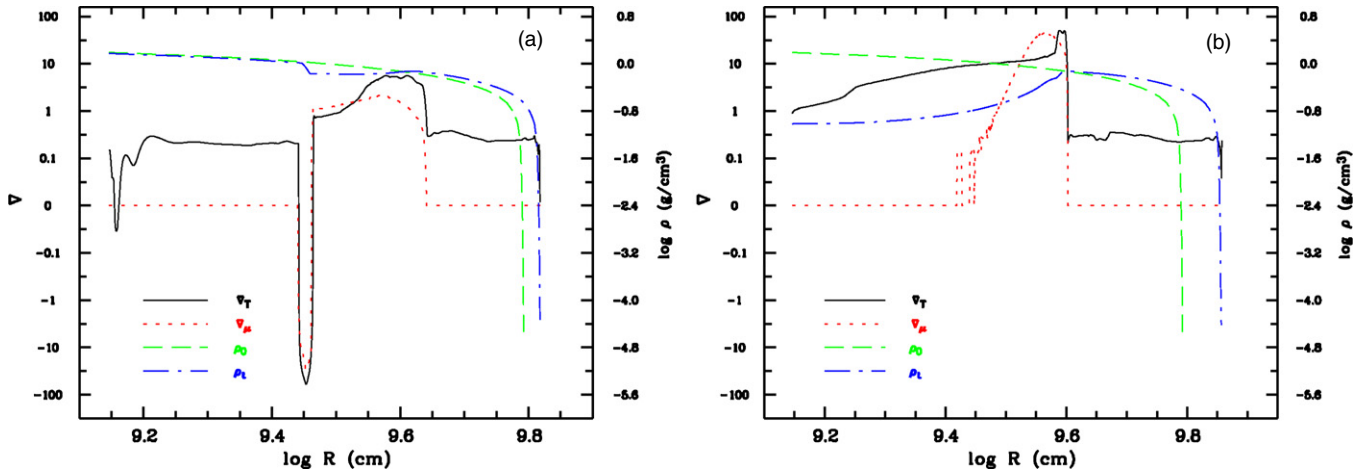


Figure 2. Gradients for temperature and molecular weight distributions for models Lb1 (on the left panel) and Lb2 (on the right panel) after the models have reached quasi-static equilibrium. The black solid line shows the temperature gradient. The red dotted line corresponds to the molecular weight gradient. The density profiles for both models are overplotted on the same plots. The green dashed line represents the density profile of the initial model. The blue dash-dotted line shows the density profile at the same epoch as when those gradients are plotted.

(A color version of this figure is available in the online journal.)

where the symbols denotes their usual meanings. Note that r denotes the element coordinate at some particular time which corresponds to the fluid density ρ_0 . Usually, these two values are viewed as our initial condition, while $R(r, t)$ means the coordinate at time t for the same element which initially located at r . In order to smooth the shock, we included the artificial viscosity denoted as q . Dissipation associated with the artificial viscosity is added to Equation (6) to ensure the conservation of total (kinetic, potential, and internal) energy. Since we are primarily interested in cohesive collisions and mergers with no mass loss, the gravitational potential includes only the planet's contribution.

When discretizing the equations, we use a staggered grid in space. As the code is written in Lagrangian scheme, the coordinates will change with the gas flow. Thus, the interval of the grids may become very small (for example, in the piling up region) or very large (when the gas is heated by the giant impact and expands). That would not only significantly reduce the time step but also lead to numerical inaccuracy in the solution of differentiation equations. The solution is to readjust the mesh after every time step, i.e., merging the nearby two grids when the interval becomes small and splitting one grid into two when the interval becomes unacceptably large.

During the initial evolution after each major impact, we solve the continuity and momentum equations explicitly. The time steps for the numerical integration are chosen appropriately so that the Courant condition is satisfied. In order to avoid numerical instability, we implicitly solve for the energy equation, which can be converted to the form

$$-c_v \frac{\partial T}{\partial t} + \frac{P\delta}{\rho^2\alpha} \frac{\partial \rho}{\partial t} = \frac{1}{\rho} \nabla \cdot \vec{F}. \quad (8)$$

3.2.2. Thermal Energy Transport

In the SPH scheme, the equation of state for the gas is approximated by a $\gamma = 5/3$ polytrope and also by an ideal gas equation of state. Kinetic energy is dissipated into thermal energy during the impact. Subsequently, the thermal energy is transported to the surface and the merger product contracts on a Kelvin–Helmholtz timescale.

One advantage of the LHD scheme is its versatility which allows us to incorporate various prescriptions for the equation

of state and consider the influence of phase transition, elemental separation, density, and molecular weight distribution. These effects determine whether convection may be stabilized in some regions of the envelope. The Saumon et al. (1995) equation of state is used, which especially takes into account the non-ideal effects of hydrogen at high pressure.

For the transported energy flux F in Equation (6), we considered both radiative and convective energy transfer. In the radiative regions, F is calculated using the radiative diffusion equation with a flux limiter (Burkert et al. 2005). For opacity, we include the contribution from grains which are generally several orders of magnitude larger than that from gas molecules (Alexander & Ferguson 1994).

In our LHD, convection is calculated using the standard mixing length prescription (Kippenhahn & Weigert 1990). In the quasi-hydrostatic planetary structure models developed by Pollack et al. (1996), convection is assumed to be efficient and the gas attains an adiabatic state throughout the envelope. This assumption is adequate in the envelope of present-day gas giants where the density is sufficiently high for convection to be effective. However, in the simulation of giant impacts, the envelope may expand greatly to attain a low-density state in which convection is unlikely to be efficient (see Figure 2). Therefore, we adopt the more realistic mixing-length treatment for the convection during both expansion and quasi-steady contraction phases. This effect is important in determining the rate of radiation transfer, the extent of envelope expansion, and the rate of planetary contraction.

In contrast to the prescription developed by Wuchterl (1991), we apply the standard mixing length prescription under the assumption that the background gas is in a quasi-hydrostatic equilibrium state. This approximation is adequate for the stage during which the magnitude of the radial velocity of the gas ($|u|$) is smaller than the convective speed V_{con} . However, during the dynamical transition phase after a giant impact, the expansion of the envelope is supersonic over some regions of the envelope and the efficiency of convection may fall below that estimated with the mixing length prescription. Although the validity of the mixing length prescription is weakened, it does provide an upper limit on the rate of energy loss and a lower limit on the extent of the envelope's expansion.

3.2.3. Initial Parameters for the LHD Models

We assume that the planet is initially in a hydrostatic equilibrium. In order to construct an initial model for a gas giant planet, we use Runge–Kutta integration method to generate the internal structure of the planet. In these calculations, constant entropy is assumed to represent efficient heat transport in the convection zone.

The initial model is relevant for a planet with a total mass $M_p = 100 M_\oplus$ and radius $R_p = 6.2 \times 10^9$ cm. It contains a core with $M_{\text{core}} = 10 M_\oplus$ and $R_{\text{core}} = 2.2 R_\oplus$. The surface temperature of this planet is set to be $T_e = 150$ K. Such a model corresponds to a long-period gas giant planet with an equilibrium temperature at around 5 AU from a solar-type star. These initial conditions are similar to those used in the SPH simulations.

Starting with these initial conditions, we further evolve the model for a few years and compare our results with those obtained by planetary structure and evolution method (under the assumption of hydrostatic equilibrium, cf. Pollack et al. 1996). This computed duration is long compared to the dynamical timescale but short compared with Kelvin–Helmholtz timescale. Although the results obtained with these two prescriptions agree well in the dense inner envelope, they differ slightly in the outer tenuous regions. The main cause for this difference is that convection is unlikely to be efficient in the low-density outer regions. Although such an approach is more time consuming, we adopt a more realistic mixing length prescription for our LHD models.

4. LHD SIMULATIONS OF GIANT IMPACT AND MERGER OF GAS GIANTS

The results of SPH simulations show complex flow patterns during giant impacts of embryos with gas giants and during mergers of two gas giant planets. In a few dynamical times, the structure of the core and gaseous envelope quickly restores to spherical symmetry during head-on collisions. In this limit, we utilize the LHD scheme to study the evolution of the GIM products' structure over a larger dynamical range.

In this series of simulations, we adopt the same model parameters as we used to simulate head-on parabolic collisions with the SPH scheme. As expected (and illustrated in Section 3.1), after initial transitions, spherical symmetry is rapidly re-established. SPH simulations also indicate that relatively large protoplanetary cores can survive passage through the gas giant's envelope and merge with the core. Based on these results, our one-dimensional LHD is sufficient to simulate the head-on GIMs.

The results of three sets of simulations are summarized in Table 1 marked as “L.” They are three sets of models in which the impactor is a $25 M_\oplus$ protoplanetary core, a $10 M_\oplus$ protoplanetary core, and a Saturn-mass gas giant. All of these models are assumed to be in hydrostatic equilibrium prior to the impact. From virial theorem (Kippenhahn & Weigert 1990), we find that the total energy for a polytropic equation of state is

$$W = E_g + E_i = (\zeta - 1)E_g/\zeta, \quad (9)$$

where E_g and E_i are gravitational binding and internal energy, $\zeta = 3(\gamma - 1)$. For $\gamma = 5/3$, $E_i = -E_g/2$. At the onset of the simulation, we impose a burst of thermal energy, $E_a = M_I v_{\text{imp}}^2/2$, in order to take into account the energy released in the vicinity of the core. Therefore, the total energy becomes $W' = E_a - E_g/2$. We also adopt the assumption that the cores

and embryos are completely merged during the head-on impacts. This assumption is supported by the results of SPH models Sa, Sb, and Sc.

For a impactor with mass of $M_I = 25 M_\oplus$, a parabolic collision (model La) leads to a merger without any loss of the gaseous envelope. The gas giant's photospheric radius expanded slightly. Analogous dynamical parameters are imposed for a $10 M_\oplus$ impactor. In this case, the gaseous envelope is heated by the impact energy and the interior temperature is increased by an order of magnitude. However, the gravity of the gas giant is also increased due to the accretion of a $10 M_\oplus$ protoplanetary core. Therefore, the expansion of the envelope due to the impact heating is suppressed and the gas giant contracted a little bit for this model. In model Lb, the asymptotic radius after the impact is in fact slightly smaller than its initial radius as a consequence of the increase in the core mass. In the parabolic model Lc, the merger product produces a much larger photospheric radius than the gas giants' initial size. Nevertheless, the entire envelope is retained due to a comparable increase in the merger's thermal and gravitational binding energy.

4.1. Mixing of Cores and Envelope Material

In the discussion above and in Section 3.1, we showed with SPH that the impactors with masses of $10 M_\oplus$ and $25 M_\oplus$ had adequate mass and intruding velocity to reach the core of the target planet without total disruption. In this subsection, we consider the mixing between the two cores and that between the core and the envelope. The efficiency of mixing determines the evolution of the merger's internal structure and mass–radius relation.

Massive impactors have $M_{I,c}$'s which are significant fractions of or comparable to the $M_{T,c}$. The dissipated energy E_a is comparable to the gravitational binding energy of the target gas giant. If this energy is efficiently converted to thermal energy throughout the merged core, the temperature in the core would increase by

$$\begin{aligned} \Delta T_{\text{core}} &\simeq (\gamma - 1)(\mu/R_g)(E_a/M_{f,c}) \\ &\sim (v_{\text{imp}}/v_{\text{esp}})^2 T_i (M_{i,c}/M_{f,c}), \end{aligned} \quad (10)$$

where T_i is the core temperature prior to the impact.

In the model La, $\Delta T_{\text{core}} > 5 \times 10^4$ K which is most likely to be larger than that (T_{evap}) for heavy elements to fully evaporate into a gas phase. In this limit, the vapors of heavy elements would thoroughly mix with the nearby hydrogen gas in the envelope. In the SPH models, the core and the embryos are approximated as fluids with the Tillotson (1962) equation of state for iron and basalt.

At lower temperatures, the mixture of composite elements undergoes phase separation. Although the phase separation diagram is well established for the H-He mixtures (Stevenson 1976), its analogs for the H-Fe or H-Basalt mixtures are not available. Nonetheless, we expect the heavy elements in the gas phase to separate from hydrogen into a two-phase medium as the temperature decreases below a critical value T_{2p} . During the phase separation, there is an exchange between Gibbs free energy and the internal energy E_i (Stevenson 1976).

After phase separation, density contrast between the two phases increases with additional reduction in temperature. If the heavy elements can assemble liquid drops centered around the nucleation sites and grow to sufficiently large sizes, they would precipitate and settle to the core (nucleation is a poorly understood critical phenomenon and it can proceed

over a considerable timescale). Further reduction in the planet's internal temperature below some threshold T_{cond} would lead to the condensation of the heavy elements (Hubbard 1984).

4.2. Core Growth After Impactor's Disintegration in the Envelope

We consider that for less massive ($M_I \lesssim$ a few M_{\oplus}) impactors, especially for oblique collisions, the impactors may disintegrate before reaching the core. The distribution of heavy elemental deposition dM_{dep}/dr depends on the impact angle, internal density inside the gas giant, and the mass of the impactor. Without the loss of generality, we adopt a simple algebraic expression such that the rate of density added at each radius is

$$\frac{\partial \rho_{\text{dep}}(r)}{\partial t} = \frac{\rho_{\text{nor}}}{\tau_{\text{dep}}} \left(1 - \left(\frac{r - r_{\text{dep}}}{\Delta r_{\text{dep}}} \right) \right)^{\eta} \exp \left(-\frac{t - t_{\text{imp}}}{\tau_{\text{dep}}} \right), \quad (11)$$

where t_{imp} and τ_{dep} represent the epoch of the impact and the duration of disintegration, r_{dep} and Δr_{dep} correspond to the main and spread in the location of disintegration, η is a power index which describes the confinement of disintegration, and ρ_{nor} is a normalization factor for matching the impact's total mass. The actual value of r_{dep} is determined by the disintegration condition, which may have a wide dispersion due to different impact trajectories and collisional speeds even for the embryos with similar masses.

After the disintegration is completed, $dM_{\text{dep}}/dr = 4\pi \int r^2 (\partial \rho_{\text{dep}}(r)/\partial t) dt$. The associated energy dissipation rate is

$$\frac{\partial^2 E_{\text{dep}}(r)}{\partial r \partial t} = \frac{GM_p(r)}{r} \frac{\partial^2 M_{\text{dep}}}{\partial r \partial t} \quad (12)$$

and change in the local temperature is

$$\Delta T_{\text{dep}} \simeq \frac{\gamma - 1}{R_g} \mu' \frac{GM_p(r)}{(M_{\text{dep}}/dr + 4\pi \rho r^2)r} \frac{dM_{\text{dep}}}{dr}, \quad (13)$$

where

$$\mu' = (\mu_{\text{dep}}(dM_{\text{dep}}/dr) + \mu_{\text{env}} 4\pi \rho r^2) / (M_{\text{dep}}/dr + 4\pi \rho r^2) \quad (14)$$

is the modified molecular weight.

Depending on the model parameters, the magnitude of ΔT may not be adequate for the new temperature to reach T_{2p} . In that case, the heavy elements retain their own identities in the form of emulsions. Around the nucleation site, heavy elements congregate and form droplets. Due to the buoyancy effect, these droplets (with density ρ_d greater than the local gas density ρ_g) have a tendency to precipitate. In a convective region where the local convection speed is v_{conv} , droplets with sizes s larger than a critical size

$$s_{\text{settle}} \sim \rho_g v_{\text{conv}}^2 / \rho_d g \quad (15)$$

(where g is the local gravity) would sediment with a speed

$$v_{\text{settle}} \sim (s/s_{\text{settle}})^{1/2} v_{\text{conv}} \sim (sg\rho_d/\rho_g)^{1/2}. \quad (16)$$

Smaller droplets may also be dragged by the convective eddies, diffuse to and become part of the core.

The actual size distribution of the droplets may depend on not only how the impactors break up but also how their fragments subsequently interact with the ambient gas in the envelope. Equation (11) is based on the assumption that the impactor is completely disintegrated down to the molecular scales which

then form liquid droplets around the nucleation sites. These liquid droplets coagulate as they collide through dispersive motion or differential settling. They also fragment due to both collisional fragmentation as well as Kelvin–Helmholtz and Rayleigh–Taylor instabilities at their interfaces with the envelope gas. For sufficiently small droplets, these instabilities are stabilized by their surface tension. Sublimation (from liquid to gas phase), condensation (from liquid to condensed state), chemical reaction, and sedimentation can also contribute to the size distribution.

Despite all these uncertainties, we consider a general power-law size distribution in which $dN/ds \propto s^{\lambda}$. For solid particles in a gas free environment, collisional equilibrium is established with $\lambda \sim -3.5$ (Dohnanyi 1969; Williams & Wetherill 1994; Farinella & Davis 1996; Tanaka et al. 1996; Kenyon 2002; Weidenschilling 2004).

The SPH models presented in Section 3.1 show that differentiation occurs rapidly. This evolution is possible if the heavy elements can concentrate into large coherent clouds. However, these results may be an artefact of the SPH scheme which uses a separate set of independent “fluid particles” to represent the hydrogen gas. This scheme does not take into account the Gibbs free energy associated with the mixing of two species. On the scale of the individual fluid elements, they are not subject to additional fragmentation. Since this scale is $\gg s_{\text{settle}}$, sedimentation speed becomes a significant fraction of v_{esc} and the timescale for differentiation becomes comparable to that for dynamical collapse.

In principle, the sedimentation of the disintegrated debris should be analyzed with a two fluid approach. However, if the fragments are sufficiently small to be well coupled to the gas, the flow can treat the mixture as one gas with a modified molecular weight μ' . With Equations (11), (12), and (14), we include the effect of energy deposition, mass loading, and molecular weight increases in the LHD models.

In order to simulate an event in which an embryo disintegrates in the planet's envelope, we introduce a new model Lb1. All the initial and boundary conditions in this model are identical to those of model Lb, except we set $r_{\text{dep}} = 2r_{\text{core}}$, $\Delta r_{\text{dep}} = 0.3r_{\text{dep}}$, and $\tau_{\text{dep}} = 10^6$ s in Equation (11). The normalization factor ρ_{normal} is adjusted so that the total mass of the impactor remains to be $10 M_{\oplus}$. The associated $E_a = 2.4 \times 10^{41}$ erg which is similar to that (2.22×10^{41} erg) for model Lb.

In model Lb1, debris of the impactor is deposited well outside the target gas giant's core. Over a few dynamical timescales, a quasi-hydrostatic equilibrium is established in the envelope and the flow speed everywhere inside the photosphere decreases below $0.1 c_s$. Thereafter, the planet's interior structure evolves through thermal adjustments as heat is transferred from its interior and lost near its photosphere. The efficiency of heat transfer is determined by not only radiative diffusion but also thermal convection.

According to the standard Schwarzschild criterion, the chemically homogeneous planetary envelope is generally unstable against convection. However, heavy element and energy deposition after a major impact modify the local thermal and compositional distribution. According to the Ledoux criterion, the flows can be stabilized by the molecular weight gradient if

$$\nabla_T < \nabla_{ad} + (\varphi/\delta)\nabla_{\mu}, \quad (17)$$

where the radiative $\nabla_T = (P/T)(dT/dP) = (3\kappa F/4acT^2)(P/g)$, the adiabatic $\nabla_{ad} = (\gamma - 1)/\gamma \sim 0.4$, and chemical $\nabla_{\mu} = (d \ln \mu / d \ln P)_s$. The subscript s refers to the surrounding

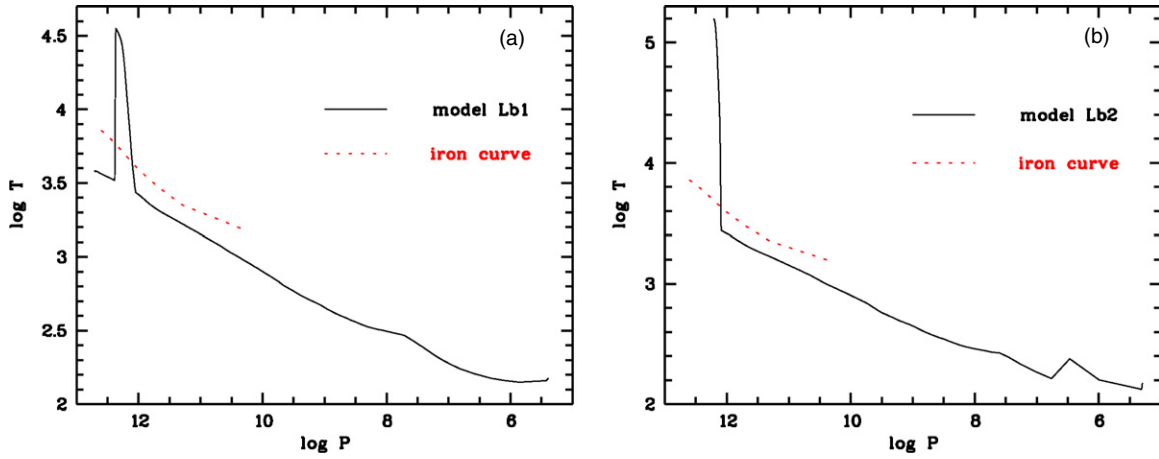


Figure 3. P–T diagrams for models Lb1 (on the left panel) and Lb2 (on the right panel). Overplotted is the melting curve of iron. (A color version of this figure is available in the online journal.)

medium. For an ideal gas, both $\varphi(\equiv d\ln\rho/d\ln\mu)$ and $\delta(\equiv -d\ln\rho/d\ln T)$ equal to unity (Kippenhahn & Weigert 1990).

The initial density distribution for model Lb1 is plotted on the left panel of Figure 2. Along with the density distribution, overplotted are the ∇_T , and ∇_μ distribution shortly after a quasi-hydrostatic equilibrium is reached. At this epoch, there are three interesting regions.

1. Outside $r = 3.3 \times 10^9$ cm, the envelope is convectively unstable because both the Schwarzschild and Ledoux criteria for stability are not satisfied. The impulsive heat deposition drives vigorous convection to transport heat and to mix the heavy elements with the envelope gas.
2. In the region $r = 3 \times 10^9 - 3.3 \times 10^9$ cm, where the Ledoux criterion for stability is satisfied but the Schwarzschild criterion is not, the envelope is dynamically stable but vibrationally unstable (or over-stable) (Kippenhahn & Weigert 1990). In this limit, double (thermal and chemical) diffusion leads to layered structure in which diffusive radiative layers are sandwiched between convective layers which are well mixed and have adiabatic structures. When averaged over many layers, stratification would probably adjust toward a state of marginal stability. With an equation of state, $d\rho/\rho = \alpha(dP/P) - \delta(dT/T) + \psi(d\mu/\mu)$, the Ledoux criterion is marginally satisfied with

$$\nabla_{\text{tot}} = \nabla_{\text{rad}} - \nabla_{\text{adiabatic}} - \nabla_\mu(\psi/\delta) \simeq 0. \quad (18)$$

3. Interior to $r = 3 \times 10^9$ cm, the flow is stable according to both criteria and the initial convective envelope is stabilized by the heat released and heavy element deposition.

In both regions 2 and 3, convection is suppressed with vanishing v_{conv} . After the impact, the temperature in these regions is well above T_{cond} (see Figure 3, panel (a)) and most likely above T_{2p} . Despite the stabilization of regions 2 and 3 against convection, heat is still transferred to the planet’s surface through radiative diffusion. On a much longer Kelvin–Helmholtz cooling timescale (~ 10 – 100 Myr), phase separation would lead to the formation of liquid droplets when the envelope’s temperature declines below T_{2p} , provided that the condition allows the conversion of Gibbs free energy to internal energy.

Droplets grow through condensation and coagulation. While the convective stability is maintained, relatively large droplets

would sediment toward the core with a terminal speed $v_{\text{settle}} \sim (sg\rho_d/\rho_g)^{1/2} \sim (s/R_p)^{1/2}v_{\text{esc}}$. In this Stoke’s range, the sedimentation timescale ($\tau_{\text{settle}} \sim (R_p/s)^{1/2}\tau_{\text{dyn}}$, where $\tau_{\text{dyn}} \sim (R_p^3/GM_p)^{1/2}$ is the dynamical timescale) is shorter than the age of mature solar-type star, τ_* .

Drag on the small particles (with $s < s_{\text{mfp}}$, where the mean free path $s_{\text{mfp}} \simeq 5 \times 10^{-9} \text{ cm}/(\rho/1 \text{ g cm}^{-3})$ for the ambient hydrogen gas) is in the Epstein range. In this limit, $v_{\text{settle}} \sim (sg/c_s)(\rho_d/\rho_g) \sim (s/R_p)v_{\text{esc}}$ and $\tau_{\text{settle}} \sim (R_p/s)\tau_{\text{dyn}}$ which may be substantially longer than τ_* .

The above consideration indicates that the debris deposit of moderate-mass embryos which disintegrated in the planetary envelopes not only introduces a metal-enriched layer well outside the core but also locally suppresses convection. These two effects promote fragment sedimentation and the growth of their cores.

4.3. Core Erosion After Impactor’s Disruption Near the Core

It has long been recognized that compositional stabilization is an important process in preserving the heavy-element-rich cores against thermal convection of the gaseous envelopes in isolated gas giants (Guillot et al. 2004). If turbulence in the convective envelopes can reach the cores, mixing and erosion would reduce $M_{t,c}$. However, this diffusion leads to a strong negative molecular weight gradient across the core-envelope interface. This gradient would quench thermal convective instabilities, suppress the compositional diffusion rate, and preserve the core-envelope separation.

In Section 3.1 and Section 4, we showed that in nearly head-on GIMs, sufficiently massive impactors can penetrate deeply into the target gas giants’ envelopes and reach their cores. For these GIMs, we show in this subsection that the impulsive dissipation of impact energy would strongly drive thermal convection despite the compositional gradient introduced by the heavy element injection and diffusion.

In order to demonstrate this possibility, we construct model Lb2, in which debris of the impactor is deposited in the proximity of the target gas giant’s core. All the initial and boundary conditions in this model are identical to those of model Lb, except we set $r_{\text{dep}} = r_{\text{core}}$, $\Delta r_{\text{dep}} = 0.25r_{\text{dep}}$, and $\tau_{\text{dep}} = 1 \times 10^6$ s in Equation (11). The normalization factor ρ_{normal} is adjusted so that the total mass of the impactor remains to be $10 M_\oplus$. The associated $E_a = 1.61 \times 10^{41}$ erg.

Similar to model Lb1, a quasi-hydrostatic equilibrium is established in the envelope and the flow speed everywhere decreases below $0.1 c_s$ after a few dynamical timescale. We plot ρ_g , ∇_T , and ∇_μ distribution at this epoch for model Lb2 on the right panel of Figure 2. By this stage, a fraction of the debris of the disintegrated impactors has reached $r = 4 \times 10^9$ cm. Within this radius, both the Schwarzschild and Ledoux criteria for stability are violated and the heat release near the core strongly enhances the tendency for thermal convection throughout the envelope, including the boundary layer region.

The subsequent evolution of the heavy elements depends on whether the collisions lead to a total phase transition of the core. Let us first consider the possibility of a hot core with an initial temperature $T_{\text{core}} > T_{\text{cond}}$ so that the heavy elements are in a liquid or gas state. Provided the core-envelope interface is stabilized by an initial compositional gradient in accordance with the Ledoux criterion, this differentiated structure would be preserved.

After the impact, vigorous and efficient convection would induce the interior of the planet to evolve toward a new constant-entropy state. During that evolution, if a fraction of the dissipated energy $f E_a$ is transported into the central region, the fractional change in the core would be $\Delta T_{\text{core}}/T_{\text{core}} \sim f E_a/E_i$ (In the limit $E_a > E_i$, ΔT_{core} would be given by Equation (10)). The timescale for thermal adjustment toward this state is approximately

$$\tau_{\text{ad}} \sim f E_a / 4\pi R_{\text{core}}^2 F_{\text{core}}, \quad (19)$$

where F_{core} is the rate of heat transport into the core (In the limit of high heat conduction rate, F_{core} would be the convection flux near the core radius R_{core} and it can be computed using standard mixing length prescription). During this time, the amount of heat loss from the planetary surface is $\sim 4\pi R_p^2 F_{\text{sur}}$ where F_{sur} is the planet's intrinsic heat flux at its surface (note that F_{sur} does not include the reprocessed stellar irradiation). From energy conservation, we find $f \sim (1 + (F_{\text{sur}}/F_{\text{con}})(R_p/R_{\text{core}})^2)$.

With sufficient input energy E_a , the core temperature can increase above T_{evap} so that the heavy elements are evaporated. In the limit of efficient convection, the envelope's temperature distribution adjusts to establish constant entropy state. Heavy element would mix with the gas in regions where the local temperature is above T_{2p} . If this radius extends well beyond the initial R_{core} , a substantial fraction of the core would be eroded and mixed with the envelope. However, if after the impact, $T'_{\text{core}} = T_{\text{core}} + \Delta T_{\text{core}} < T_{\text{evap}}$ or the region with $T > T_{2p}$ is confined to small radius, the core structure would be mostly preserved even though convection may be able to penetrate through the initial core-envelope interface.

We now consider the possibility of GIMs onto gas giants with cool ($T_{\text{core}} < T_{\text{cond}}$) cores. With sufficiently massive and energetic impactors, head-on collisions lead to $T'_{\text{core}} > T_{\text{evap}}$. The subsequent evolution is similar to that discussed above, albeit a modest fraction of internal energy must be used to compensate for the latent heat during the melting and evaporation of the core. Less energetic impacts may not be able to evaporate the core, in which case the temperature distribution of the core would be determined by the energy Equation (8) including heat transport by conduction. Provided the new $T > T_{\text{cond}}$ at the core-envelope interface, the molten heavy elements would be entrained into the convective eddies on the growth timescale for Kelvin–Helmholtz instability. This rate may be limited by the poorly determined material properties such as surface tension and phase separation. However, if $T > T_{2p}$ at the core-envelope

interface, mixing between the heavy elements and hydrogen may be much more efficient. Since convection in the envelope extends to the interface, the mixed gas is redistributed throughout the convective region with $T > T_{2p}$.

5. SUMMARY AND DISCUSSIONS

The main objective of this paper is to suggest that giant impacts and merger process may have led to different core-envelope structure between Jupiter and Saturn and the super-solar metallicity in their gaseous envelopes.

We have highlighted several avenues of GIMs by embryos onto gas giants. The supply of these large solid building blocks include *in situ* embryos during the final phase of gas giant formation and terrestrial bodies cleared by sweeping secular resonances and dynamical instabilities. There are also several processes which can lead to the merger of gas giants, including orbit crossing triggered by runaway migration, and long-term dynamical instability.

At their present-day orbits, the velocity dispersion of any residual embryos or planetesimals is less than the gas giants' surface escape speed. The GIMs between any residual planetesimals, embryos, or hypothetical gas giants and long-period gas giants are likely to be parabolic and attain limited amount of energy. This modest velocity dispersion also enlarges gas giants' gravitational cross section.

The discussions above indicate that embryos with a mass of several M_{\oplus} can penetrate through the envelope and reach the core of gas giants through head-on collisions. If these collisions are sufficiently energetic, they would lead to significant core erosion. Heavy elements would be well mixed with the hydrogen in the envelope down to a molecular level. The average density and metallicity of the gas in the envelope would be enhanced. Although a relatively large amount of kinetic energy is dissipated into internal energy, the heat released from this type of GIM is efficiently transported to the planet's surface and radiated away because the envelope is fully convective.

Low-mass impactors ($M_I \ll M_{\oplus}$) are likely to disintegrate in gas giants' envelopes. Energy deposition in the planet's envelope suppresses convection interior to r_{dep} . Heavy element deposition also increases the opacity. After the planet has adjusted to a new hydrostatic equilibrium, the impact dissipation energy is more effectively retained by the reduced heat flux through the envelope. Suppression of convection also leads to sedimentation of modest to large size embryos. In the limit that a collisional equilibrium can be established with most of the debris' mass being in the forms of large particles, the core attains, from the post-impact differentiation, a mass substantially larger than the critical mass (a few M_{\oplus}) for the onset of efficient gas accretion (Pollack et al. 1996; Ida & Lin 2004).

We suggest that these two limiting cases introduce diversity in the core-envelope structure. They may also lead to different cooling rates during the subsequent thermal evolution. For the core-impact case, the dredge-up of heavy elements does not suppress convection. During the cooling process, phase separation and phase transition lead to changes in the Gibbs free energy which may lead to the release of additional sources of internal energy to reduce the planet's contraction rate. For the envelope-disintegrate case, small grains or droplets are the dominant sources of opacity (de Pater & Lissauer 2001) and their suspension or depletion determines the contraction rate of the gas giant. Analysis for the long-term thermal evolution of planets will be considered and presented elsewhere.

We suggest that Jupiter may have been struck by an energetic head-on GIM which penetrated deeply into its envelope and led to its core erosion. With a larger ($> 10 M_{\oplus}$) initial core, it would also partly resolve a long standing issue on how Jupiter might acquire its massive gaseous envelope with such a small core on the multi-Myr timescale over which their natal solar nebula is depleted.

In contrast, Saturn may have acquired its present large core through GIMs with less energetic and smaller residual embryos. A temporary stabilization of Saturn's envelope against convection may have also prolonged its contraction timescale and enabled the precipitation of helium dropout in its envelope. We note that both processes lead to the enrichment of metallicity in the envelopes of Jupiter and Saturn.

GIMs are most likely to occur within the first few Myr of their life span. Energy dissipation from such events is likely to increase the intrinsic luminosity and radius of these planets. Direct imaging and rare transit observations may provide observational verifications that the internal structure of typical gas giants may have been modified by GIMs. We shall discuss the GIM's influence on the mass-radius-luminosity of the close-in planets in Paper II.

We have shown possible mechanisms for the dredge up of heavy elements from the core and for the promotion of core growth. We have not considered here the long-term sustainability of the stir-up elemental distribution. The follow-up evolution of the impacted gas giant's radius depends sensitively on their cooling efficiency and elemental segregation. Although there are models for contraction and differentiation of initially homogeneous gas giants (Bodenheimer et al. 2003; Baraffe et al. 2008), the long-term post GIM evolution still needs to be investigated.

We thank Drs P. Bodenheimer, P. Garaud, T. Guillot, and G. Laughlin for useful conversation. Part of the calculation was carried out on the SG1 Altix 330 system at the Department of Astronomy, Peking University. This work is supported by NASA NNX07A-L13G, NNX07AI88G, NNX08AL41G, NNX08AM84G, and NSF(AST-0908807). C.B.A.'s involvement was supported by NASA (NNG05G1496).

REFERENCES

- Agnor, C., & Asphaug, E. 2004, *ApJ*, **613**, L157
- Alexander, D. R., & Ferguson, J. W. 1994, *ApJ*, **437**, 879
- Alibert, Y., Mordasini, C., & Benz, W. 2004, *A&A*, **417**, L25
- Anic, A., Alibert, Y., & Benz, W. 2007, *A&A*, **466**, 717
- Asphaug, E., Agnor, C. B., & Williams, Q. 2006, *Nature*, **439**, 155
- Asphaug, E., Ostro, S. J., Hudson, R. S., Scheeres, D. J., & Benz, W. 1998, *Nature*, **393**, 437
- Balbus, S. A., & Hawley, J. F. 1991, *ApJ*, **376**, 214
- Baraffe, I., Chabrier, G., & Barman, T. 2008, *A&A*, **482**, 315
- Benz, W. 1990, in NATO ASI Ser. C 302, Numerical Modelling of Nonlinear Stellar Pulsations Problems and Prospects, ed. J. R. Buchler (Dordrecht: Kluwer), 269
- Benz, W., Anic, A., Horner, J., & Whitby, J. A. 2007, *Space Sci. Rev.*, **132**, 189
- Benz, W., & Asphaug, E. 1999, *Icarus*, **142**, 5
- Benz, W., & Hills, J. G. 1987, *ApJ*, **323**, 614
- Benz, W., Slattery, W. L., & Cameron, A. G. W. 1986, *Icarus*, **66**, 515
- Benz, W., Slattery, W. L., & Cameron, A. G. W. 1988, *Icarus*, **74**, 516
- Bodenheimer, P., Hubickyj, O., & Lissauer, J. J. 2000, *Icarus*, **143**, 2
- Bodenheimer, P., Laughlin, G., & Lin, D. N. C. 2003, *ApJ*, **592**, 555
- Bodenheimer, P., & Pollack, J. B. 1986, *Icarus*, **67**, 391
- Bryden, G., Lin, D. N. C., & Ida, S. 2000a, *ApJ*, **544**, 481
- Bryden, G., Różyczka, M., Lin, D. N. C., & Bodenheimer, P. 2000b, *ApJ*, **540**, 1091
- Burkert, A., Lin, D. N. C., Bodenheimer, P. H., Jones, C. A., & Yorke, H. W. 2005, *ApJ*, **618**, 512
- Burrows, A., Guillot, T., Hubbard, W. B., Marley, M. S., Saumon, D., Lunine, J. I., & Sudarsky, D. 2000, *ApJ*, **534**, 97
- Burrows, A., Hubeny, I., Hubbard, W. B., Sudarsky, D., & Fortney, J. J. 2004, *ApJ*, **610**, L53
- Cameron, A. G. W., & Ward, W. R. 1976, Lunar and Planetary Institute Science Conference Abstracts, **7**, 120
- Cumming, A., Butler, R. P., Marcy, G. W., Vogt, S. S., Wright, J. T., & Fischer, D. A. 2008, *PASP*, **120**, 531
- Cuzzi, J. N., & Zahnle, K. J. 2004, *ApJ*, **614**, 490
- de Pater, I., & Lissauer, J. J. 2001, Planetary Sciences (Cambridge: Cambridge Univ. Press)
- Dobbs-Dixon, I., Li, S.-L., & Lin, D. N. C. 2007, *ApJ*, **660**, 791
- Dodson-Robinson, S. E., Willacy, K., Bodenheimer, P., Turner, N. J., & Beichman, C. A. 2008, arXiv:0806.3788
- Dohnanyi, J. W. 1969, *J. Geophys. Res.*, **74**, 2531
- Duncan, M., Quinn, T., & Tremaine, S. 1987, *AJ*, **94**, 1330
- Farinella, P., & Davis, D. R. 1996, *Science*, **273**, 938
- Gammie, C. F. 1996, *ApJ*, **457**, 355
- Guillot, T., Stevenson, D. J., Hubbard, W. B., & Saumon, D. 2004, in Jupiter. The Planet, Satellites, and Magnetosphere, ed. F. Bagenal, T. E. Dowling, & W. B. McKinnon (Cambridge: Cambridge Univ. Press), 35
- Hahn, J. M., & Malhotra, R. 1999, *AJ*, **117**, 3041
- Hartmann, W. K., & Davis, D. R. 1975, *Icarus*, **24**, 504
- Helled, R., Podolak, M., & Kovetz, A. 2008, *Icarus*, **195**, 863
- Hubbard, W. B. 1984, Planetary Interiors (New York: Van Nostrand Reinhold)
- Hubickyj, O., Bodenheimer, P., & Lissauer, J. J. 2005, *Icarus*, **179**, 415
- Ida, S., & Lin, D. N. C. 2004, *ApJ*, **604**, 388
- Ida, S., & Lin, D. N. C. 2008, *ApJ*, **685**, 584
- Ikoma, M., Guillot, T., Genda, H., Tanigawa, T., & Ida, S. 2006, *ApJ*, **650**, 1150
- Inaba, S., & Ikoma, M. 2003, *A&A*, **410**, 711
- Kenyon, S. J. 2002, *PASP*, **114**, 265
- Kippenhahn, R., & Weigert, A. 1990, Stellar Structure and Evolution (Berlin: Springer)
- Korycansky, D. G., & Zahnle, K. J. 2005, *Planet. Space Sci.*, **53**, 695
- Kretke, K. A., & Lin, D. N. C. 2007, *ApJ*, **664**, L55
- Lesur, G., & Ogilvie, G. I. 2010, *MNRAS*, **404**, L64
- Lin, D. N. C., & Ida, S. 1997, *ApJ*, **477**, 781
- Lin, D. N. C., & Papaloizou, J. C. B. 1979, *MNRAS*, **186**, 799 (or 188, 191)
- Lin, D. N. C., & Papaloizou, J. C. B. 1980, *MNRAS*, **191**, 37
- Lin, D. N. C., & Papaloizou, J. C. B. 1993, in Protostars and Planets III, ed. E. H. Levy & J. I. Lunine (Tucson, AZ: Arizona Univ. Press), 749
- Lissauer, J. J. 1987, *Icarus*, **69**, 249
- Love, S. G., & Ahrens, T. J. 1996, *Icarus*, **124**, 141
- Masset, F. S. 2008, in IAU Symp. 249, Exoplanets: Detection, Formation and Dynamics, ed. Y.-S. Sun, S. Ferraz-Mello, & J.-L. Zhou (Cambridge: Cambridge Univ. Press), 331
- Masset, F. S., D'Angelo, G., & Kley, W. 2006, *ApJ*, **652**, 730
- Mayor, M., et al. 2009, *A&A*, **493**, 639
- Melosh, H. J. 1989, Impact Cratering: A Geologic Process (New York: Oxford Univ. Press), 45
- Militzer, B., Hubbard, W. B., Vorberger, J., Tamblin, I., & Bonev, S. A. 2008, *ApJ*, **688**, L45
- Monaghan, J. J. 1992, *ARA&A*, **30**, 543
- Murray, N., & Holman, M. 1999, *Science*, **283**, 1877
- Nagasawa, M., Lin, D. N. C., & Thommes, E. 2005, *ApJ*, **635**, 578
- Paardekooper, S.-J., Baruteau, C., Crida, A., & Kley, W. 2010, *MNRAS*, **401**, 1950
- Papaloizou, J. C. B., & Terquem, C. 2006, *Rep. Prog. Phys.*, **69**, 119
- Pollack, J. B., Hubickyj, O., Bodenheimer, P., Lissauer, J. J., Podolak, M., & Greenzweig, Y. 1996, *Icarus*, **124**, 62
- Queloz, D., et al. 2009, *A&A*, **506**, 303
- Rafikov, R. R. 2006, *ApJ*, **648**, 666
- Safronov, V. S. 1969, Evolution of the Protoplanetary Cloud and Formation of the Earth and Planets (Moscow: Nauka Press)
- Saumon, D., Chabrier, G., & van Horn, H. M. 1995, *ApJS*, **99**, 713
- Shiraishi, M., & Ida, S. 2008, *ApJ*, **684**, 1416
- Showman, A. P., & Guillot, T. 2002, *A&A*, **385**, 166
- Slattery, W. L., Benz, W., & Cameron, A. G. W. 1992, *Icarus*, **99**, 167
- Stevenson, D. J. 1976, PhD thesis, Cornell Univ.
- Stevenson, D. J. 1982, *Planet. Space Sci.*, **30**, 755
- Supulver, K. D., & Lin, D. N. C. 2000, *Icarus*, **146**, 525
- Tanaka, H., Inaba, S., & Nakazawa, K. 1996, *Icarus*, **123**, 450
- Tanigawa, T., & Watanabe, S. I. 2002, *ApJ*, **580**, 506
- Thommes, E., Nagasawa, M., & Lin, D. N. C. 2008, *ApJ*, **676**, 728
- Tillotson, J. H. 1962, General Atomic Reports, GA-3216
- Tsiganis, K., Gomes, R., Morbidelli, A., & Levison, H. F. 2005, *Nature*, **435**, 459

- Ward, W. R. 1981, [Icarus](#), **47**, 234
- Ward, W. R. 1997, [Icarus](#), **126**, 261
- Weidenschilling, S. J. 2004, in Comets II, ed. M. C. Festou, H. U. Keller, & H. A. Weaver (Tucson, AZ: Univ. Arizona Press), 97
- Wetherill, G. W. 1985, [Science](#), **228**, 877
- Williams, D. R., & Wetherill, G. W. 1994, [Icarus](#), **107**, 117
- Wuchterl, G. 1991, [Icarus](#), **91**, 39
- Wuchterl, G., Guillot, T., & Lissauer, J. J. 2000, in Protostars and Planets IV, ed. V. Mannings, A. P. Boss, & S. S. Russell (Tucson, AZ: Univ. Arizona Press), 1081
- Zhang, K., & Hamilton, D. P. 2007, [Icarus](#), **188**, 386
- Zhou, J.-L., & Lin, D. N. C. 2007, [ApJ](#), **666**, 447
- Zhou, J.-L., Lin, D. N. C., & Sun, Y.-S. 2007, [ApJ](#), **666**, 423